Limb reconstruction with decellularized, non-demineralized bone in a young leporine model

2015 Biomed. Mater. 10 015021

(http://iopscience.iop.org/1748-605X/10/1/015021)

Biomedical Materials

PAPER

Limb reconstruction with decellularized, non-demineralized bone in a young leporine model

RECEIVED
3 September 2014

REVISED
19 December 2014

ACCEPTED FOR PUBLICATION
30 December 2014

PUBLISHED
10 February 2015

Elliot C Pennington[1], Beatrice Dionigi[1], Fabienne L Gray[1], Azra Ahmed[1], Joseph Brazzo[1], Andrey Dolinko[1], Nathan Calderon[2], Thomas Darrah[3], David Zurakowski[1], Ara Nazarian[2], Brian Snyder[2] and Dario O Fauza[1]

[1] Department of Surgery, Boston Children's Hospital and Harvard Medical School, 300 Longwood Avenue, Boston, MA 02115, USA
[2] Department of Orthopedic Surgery, Center for Advanced Orthopedic Studies, Beth Israel Deaconess Medical Center and Harvard Medical School Boston, 330 Brookline Avenue, Boston, MA 02215, USA
[3] Nicholas School of the Environment, Duke University, 450 Research Drive, Durham, NC 27708, USA

E-mail: dario.fauza@childrens.harvard.edu

Keywords: bone substitutes, bone graft, bone repair, limb repair, pediatric limb repair

Abstract

Limb salvage from a variety of pathological processes in children is often limited by the unavailability of optimal allograft bone, or an appropriate structural bone substitute. In this study, we sought to examine a practical alternative for pediatric limb repair, based on decellularized, non-demineralized bone grafts, and to determine whether controlled recellularization prior to implantation has any impact on outcome. Growing New Zealand rabbits ($n = 12$) with a complete, critical-size defect on the left tibiofibula were equally divided into two groups. One group received a decellularized, non-demineralized leporine tibiofibula graft. The other group received an equivalent graft seeded with mesenchymal stem cells labeled with green fluorescent protein (GFP), at a fixed density. Animals were euthanized at comparable time points 3–8 weeks post-implantation. Statistical analysis was by the Student *t*-test and Fisher's exact test ($P < 0.05$). There was no significant difference in the rate of non-union between the two groups, including on 3D micro-CT. Incorporated grafts achieved adequate axial bending rigidity, torsional rigidity, union yield and flexural strength, with no significant differences or unequal variances between the groups. Correspondingly, there were no significant differences in extracellular calcium levels, or alkaline phosphatase activity. Histology confirmed the presence of neobone in both groups, with GFP-positive cells in the recellularized grafts. It was shown that osseous grafts derived from decellularized, non-demineralized bone undergo adequate remodeling *in vivo* after the repair of critical-size limb defects in a growing leporine model, irrespective of subsequent recellularization. This methodology may become a practical alternative for pediatric limb reconstruction.

1. Introduction

Pediatric long bone defects can be caused by a variety of pathological processes, commonly leading to life-long morbidity. The repair of these defects can be challenging due to the limited availability of suitably sized allografts, or bone alternatives. Autologous bone, the standard for osseous repair in other clinical settings, is typically a suboptimal option in children. This has prompted the search for suitable pediatric bone substitutes by various groups.

We have previously investigated the use of osseous grafts engineered from amniotic mesenchymal stem cells for the repair of a variety of experimental bony defects typical of neonates [1–3]. In those studies, grafts were created via the classic open systems tissue engineering paradigm, namely cellularized constructs based on synthetic scaffolds, which carries limitations in the setting of structural replacement of areas bearing significant biomechanical loads. In this study, we sought to investigate a relatively practical natural scaffold based on decellularized, non-demineralized bone as an alternative for pediatric long bone replacement, and to determine whether controlled recellularization prior to implantation had any effect on the clinical outcome.

2. Methods

This study was approved by the Boston Children's Hospital Institutional Animal Care and Use Committee under protocol #11-10-2066R.

2.1. Donor cell processing

A clone of heterologous leporine amniotic-derived mesenchymal stem cells (afMSCs) was isolated by a combination of mechanical separation and natural selection with culture media, as per methods we have previously described [2, 3]. Fluorescence-activated cell sorting analysis was used to confirm a mesenchymal progenitor identity in the representative colonies with unconjugated mouse monoclonal antibodies previously validated for use in rabbits, namely CD44 (Antigenix, Huntington Station, NY), CD45 (Antigenix), and CD90 (BD Biosciences, San Jose, CA), using the Vantage SE cell sorter (BD Biosciences). A mouse isotype immunoglobulin control was used to exclude nonspecific staining. Prior to the final expansion, cells were labeled with a green fluorescent protein (GFP) by retroviral nuclear infection after five to eight successive passages, based on methods previously described [4].

2.2. Decellularized bone graft fabrication

Tibiofibulas ($n = 12$) were obtained from six 22 week-old donor New Zealand White rabbits. After cutting to size, the scaffolds were decellularized following methods that have been previously described [5]. Briefly, grafts were washed with a high-velocity stream of water to remove marrow from the pore spaces, then incubated in phosphate-buffered saline (PBS, Mediatech, Manassas, VA) with 0.1% EDTA (Sigma-Aldrich, St. Louis, MO) for 1 h at room temperature. After a 1 h wash in PBS, the scaffolds were further washed in a hypotonic buffer consisting of 10 mM Tris and 0.1% EDTA (Sigma) overnight at 4 °C. The scaffolds were washed once more with PBS, and then incubated in a detergent solution of 10 mM Tris and 0.5% sodium dodecyl sulfate (SDS, Sigma) for 24 h at room temperature. The scaffolds were washed once again with PBS (Mediatech), and incubated in an enzymatic solution containing 50 U mL^{-1} DNAse, 1 U mL^{-1} RNAse, and 10 mM Tris (all Sigma) for 6 h at 37 °C. This was followed by six 1 h washes in PBS (Mediatech) to remove excess chemicals. Finally, the scaffolds were rinsed briefly in deionized water and freeze-dried. All washing and incubation steps were done in an orbital shaker at 300 rpm.

2.3. afMSC seeding and 3D osteogenesis

All of the scaffolds were sterilized with ultraviolet radiation for 20 min. per side within a laminar flow hood, followed by sequential washing in 1N NaOH, 70% ethanol, and sterile PBS (Mediatech). They were then divided into acellular and recellularized groups, depending on whether they underwent seeding or not with afMSCs. The recellularized scaffolds ($n = 6$; 1.2–2.0 cm long) were statically seeded with the previously isolated, GFP-labeled donor afMSCs at a density of 100 000 cells cm^{-2}. The seeded scaffolds were then transferred into 50 mL polypropylene conical centrifuge tubes (BD Biosciences, San Jose, CA), and further dynamically seeded with an additional 1.0×10^6 cells/10 mL in an osteogenic medium in a rotating bioreactor (Sarstedt, Germany) at 10 rpm in a 5% CO_2 incubator at 37 °C for 7 d prior to implantation. The osteogenic medium consisted of a high-glucose Dulbecco's modified Eagle medium (Sigma), supplemented with 5% fetal bovine serum (Invitrogen, Carlsbad, CA), 5 mmol L^{-1} b-glycerophosphate (Sigma), 50 mmol L^{-1} ascorbic acid-2 phosphate (Sigma), 100 nmol L^{-1} dexamethasone (Sigma), and triple antibiotic solution (Thermo Fisher Scientific, Waltham, MA) containing 10 000 U mL^{-1} Penicillin G, 10 mg mL^{-1} streptomycin, and 25 ug mL^{-1} amphotericin B. The acellular scaffolds ($n = 6$; 1.6–1.8 cm long) were incubated in the same culture media overnight in a 5% CO_2 incubator at 37 °C prior to implantation.

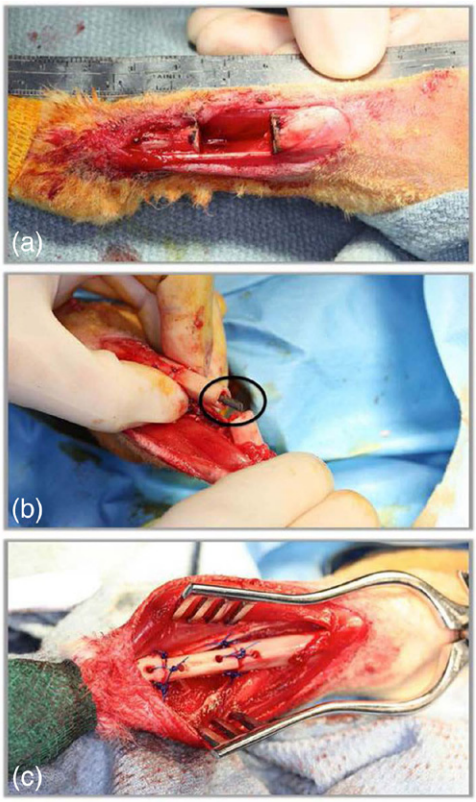

Figure 1. Intra-operative views of the creation of (*a*) a critical size tibiofibular defect; (*b*) placement of a 5 cm stainless steel intramedullary nail through the graft and across both the proximal and distal native tibiofibular; and (*c*) suturing of the graft in place through the previously drilled holes for additional stabilization.

2.4. Surgical implantation

The New Zealand White rabbits ($n = 12$, age 22 weeks) were equally divided into two groups, depending on whether an acellular or recellularized graft was used to repair the critical size-matched tibiofibular defects, surgically created on the right hind limb (figure 1). To that end, the animals were anesthetized with 1–3% isoflurane (Baxter) and given an intravenous injection of 20 mg kg^{-1} of cefazolin (Sagent) prior to surgical manipulation. The animals were prepped and draped in standard sterile fashion and a 6 cm incision was made on

Figure 2. Illustrative lateral radiograph of the repaired hind limb, immediately prior to necropsy.

the anteromedial aspect of the right hind limb, directly over the tibiofibula. The tibiofibula was then bluntly dissected circumferentially across an approximately 5 cm distance. The scaffold was used to measure a size-matched defect, which was cut using an orthopedic oscillating cast saw. After hemostasis was achieved, a handheld cordless drill was used to create three holes in the proximal and distal native tibiofibula remnants. A 5 cm stainless steel intramedullary nail was inserted through the scaffold and across both the proximal and distal native tibiofibula, after which the scaffold was sutured in place with simple interrupted 2-0 Prolene (Ethicon) placed through the aforementioned drilled holes for additional stabilization. The wound was closed in two layers. The limb was cast with cotton cast padding and polyurethane resin-impregnated knitted fiberglass casting tape (Scotchcast Plus; 3M Health Care, Saint Paul, MN), using intra-operative radiographs to ensure proper graft and intramedullary nail positions. The cast was then wrapped with a self-adherent dressing (Vetrap; 3M) and sprayed with a foul-tasting liquid (Pig Pax; Jørgen Kruuse, Denmark) to prevent the animal from chewing it.

2.5. Post-operative care and euthanasia

The animals were allowed to recover, with post-operative pain control based on a transdermal fentanyl patch (Janssen Pharmaceuticals, Titusville, NJ). They were clinically evaluated twice daily by three independent observers. Two weeks after implantation, the animals were anesthetized with 1–3% isoflurane (Baxter) to undergo 2-view extremity radiographs, so that their hard casts could be replaced with modified Robert Jones splints. The animals were again allowed to recover.

At comparable time points between the two groups, 3–8 weeks after implantation (one animal per group at post-operative days 21, 28, 35, 42, 49, and 56), the animals were euthanized with a barbiturate overdose (Virbac, France). Anterior-posterior and lateral radiographs of the right hind limb were performed, followed immediately by a necropsy (figure 2). The entire right tibiofibula, including the implanted graft, was dissected free from the surrounding soft tissues, leaving the bony callous intact and removed *en bloc*.

2.6. Quantitative micro-CT analysis

Samples were analyzed for 3D osteogenesis by imaging using a Siemens MicroCAT II scanner (Siemens Corporation, Washington, DC) with 40 μm resolution. Data were acquired with an x-ray tube voltage of 70 kV (peak), currents of 0.500 mA, and 360 steps. A manufacturer-supplied phantom provided a linear relationship between the signal intensity and specimen density. All of the image stacks were saved in DICOM format for post-processing. The average moment of inertia (defined as $I_x = \int y^2\, dA$, where y is the distance from the x-axis to an infinitesimal area dA) for each specimen was calculated using the image cross-sections. Image analysis was performed using post-acquisition image analysis freeware (Amide, http://amide.sourceforge.net) [6]. 3D images were reconstructed using a 3D software platform (Amira; FEI Worldwide, Hillsboro, OR) (figure 3). Graft and callous density were calculated using a 1 mm^3 sample using two independent observers.

Axial compressive and tensile relationships describing the mechanical properties of rat bone as a function of micro-CT generated density were used to convert the densities to their respective compressive and tensile modulus (E) values [7, 8] (figure 4). The bending (EI) rigidity for each transaxial cross-section through the bone was calculated by summing the density-weighted area (multiplication of each infinitesimal area—pixel in this case—by its density) of each pixel by its position relative to the density weighted centroid [9]. An average bending rigidity (EI_{AVG}) was reported for each specimen.

2.7. Biomechanical testing

Both the proximal and distal unions of the grafts were tested in bending using a modified three-point bending test with a 4 mm span between each point and a loading speed of 10 mm min^{-1}. Any animals with evidence of

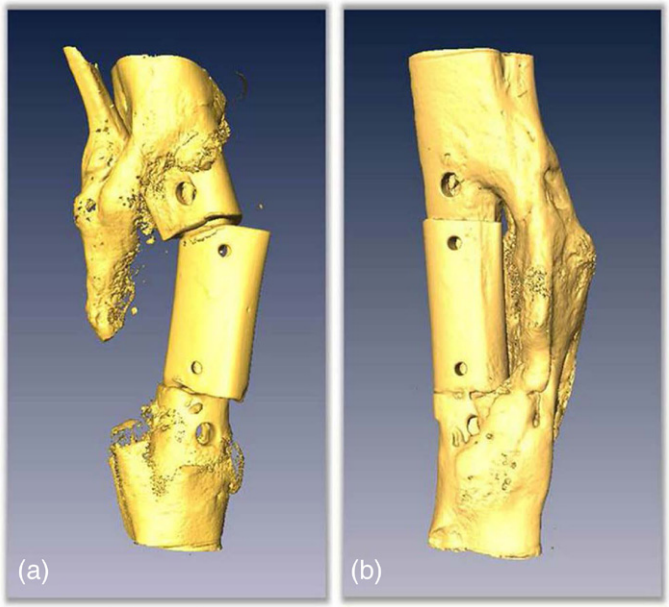

Figure 3. Illustrative 3D micro-CT images of (*a*) non-union and (*b*) union in the repaired area.

non-union were excluded from testing. The samples were loaded into a screw-driven Instron 5542 Load Frame, fitted with a 250N load cell (Instron, Norwood, MA), calibrated according to the manufacturer's instructions. Testing was conducted such that each healed section was positioned between the loading span. Displacement and load data were collected for each specimen, and the bending stress was calculated using equations for cylindrical tubes. The yield strength and flexural strength (the highest stress experienced within the material at its moment of rupture) were recorded for each specimen for both proximal and distal unions.

2.8. Biochemical analysis

Extracellular calcium deposition, an additional surrogate of construct mineralization, was measured by methods previously described [10, 11]. Briefly, samples were weighed using a microbalance (PerkinElmer, Waltham, MA). Aliquots of 0.1 mg were dried in a vacuum oven (VWR; Cornelius, OR) at 80 °C and washed at 475 °C for 24 h. Samples were crushed, digested in Teflon vessels (SCP Science, Montreal, Canada) using concentrated (15.9 mol L^{-1}) ultra-pure nitric acid (HNO_3, SCP Science) at 80 °C for 5 h, and the remaining solution was evaporated for approximately 3 h at 90 °C to remove excess nitric acid. The residual dried material was then re-digested with ultra-pure HNO_3, diluted using water purified to 18.2 MΩ cm resistance (Milli-Q Water Purification System; Millipore, Bedford, MA) to result in a final concentration of 2% nitric acid (by volume), and 10 and 1 ng g^{-1} of each of the internal standards (In and Bi) respectively. Calcium concentrations were measured using a Thermo Elemental PQIII ICP-MS (Thermo Fisher Scientific), using modifications to the EPA 6020A methodologies [11], the approved ICP-MS analytical procedure for inorganic trace elements in soils and sediments used previously for elemental analysis in bone [10, 11].

The alkaline phosphatase activity, a surrogate of active bone remodeling, was measured spectroscopically using a commercially available kit (BioAssay Systems, Hayward, CA) according to the manufacturer's instructions. Briefly, the hydrolysis of p-nitrophenol by alkaline phosphatase was determined by measuring the absorbency at 405 nm.

2.9. Histological analysis

The samples were fixed, paraffin embedded, and stained with H&E. To detect the presence of GFP-positive cells, the paraffin embedded sections were rehydrated and stained with a monoclonal GFP antibody (Clonetech, Mountain View, CA) at a dilution of 1:1500 for 60 min at room temperature, followed by blocking and secondary antibody incubation using a commercially available kit (EnVision™+; Dako, Denmark) according to the manufacturer's instructions. The precise quantification of donor cell survival *in vivo* was not possible in light of the multiple other analyses performed. Histomorphologic evaluations were performed under an EVOS® XL Core Imaging System microscope fitted with an on-board computer and integrated imaging software (Life Technologies, Carlsbad, CA).

2.10. Statistical analysis

Statistical analysis was performed using the SPSS software package version 18.0 (SPSS/IBM, Chicago, IL). The Student *t*-test and Fisher's exact test were used as appropriate, along with Levene's test to analyze variances between the groups. The statistical significance was set at two-sided $P < 0.05$.

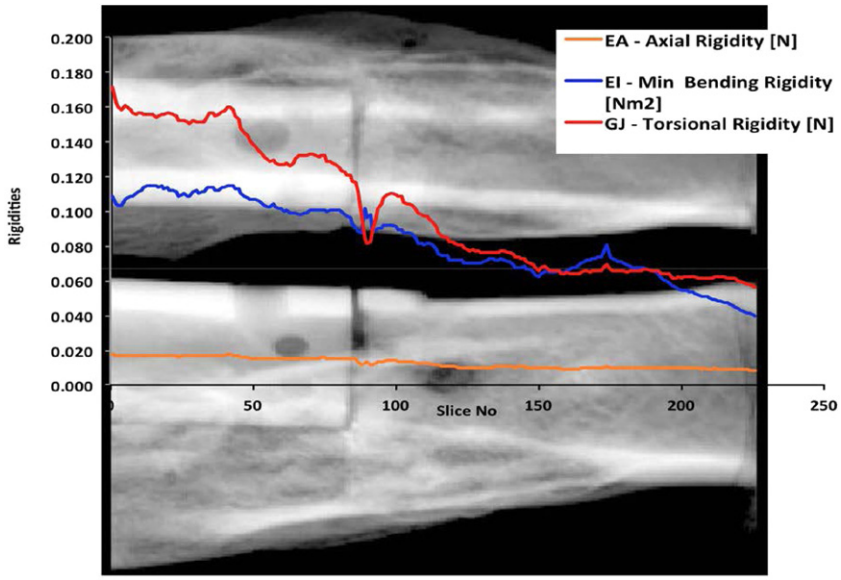

Figure 4. Biomechanical data were also measured by previously validated methods based on the shape and distribution of calcified tissue. Axial bending rigidity, minimal bending rigity, and torsional rigidity can be measured using this technique. Here, the proximal union of a single sample, seen in both the coronal and sagital planes, is superimposed with the rigidities based on the cross-sectional area.

3. Results

Intra-operative radiographs showed all of the grafts to be in good alignment with the intra-medullary nail traversing the defect. One animal in the recellularized group that developed a post-operative wound infection had to be euthanized early and excluded from the final analyses. Evidence of non-union was apparent on both gross inspection and 3D micro-CT in 2/6 (33%) of the acellular implants and in 1/5 (20%) of the recellularized grafts—this difference was not statistically significant ($P = 1.0$).

3.1. Quantitative micro-CT analysis

Except for the animals with non-unions, all of the grafts achieved adequate rigidity based on micro-CT. There were no statistically significant differences between acellular and recellularized grafts with respect to the total axial rigidity (0.009 ± 0.007N versus 0.009 ± 0.005N, $P = 0.83$), minimal bending rigidity (0.043 ± 0.034 Nm^2 versus 0.044 ± 0.027 Nm^2, $P = 0.94$), or torsional rigidity (0.056 ± 0.046N versus 0.063 ± 0.040N, $P = 0.79$). When the proximal and distal unions were analyzed separately, again no differences were found between the groups. There was a trend toward higher median density of the callous in recellularized grafts (268.3 ± 30.3 mg cc^{-1} versus 233.2 ± 50.4 mg cc^{-1}, $P = 0.21$), and of the construct in the acellular grafts (389.6 ± 62.4 mg cc^{-1} versus 333.4 ± 80.3 mg cc^{-1}, $P = 0.22$), however this did not reach statistical significance. There was no evidence of unequal variances between the groups.

3.2. Biochemical analysis

There were no significant differences between the acellular and recellularized grafts in the levels of extracellular calcium deposition of either the graft or the callous, when compared to pre-implantation levels. After adjusting for pre-implantation levels, there were no group differences with respect to time. Similarly, there was no difference in alkaline phosphatase activity between the acellular and recellularized grafts in either the callous (520 ± 404 IU $L^{-1}g^{-1}$ versus 618 ± 611 IU $L^{-1}g^{-1}$, $P = 0.76$) or the graft itself (28.7 ± 18.8 IU $L^{-1}g^{-1}$ versus 26.8 ± 17.3 IU $L^{-1}g^{-1}$, $P = 0.87$). Again, no unequal variances were found between the two groups.

3.3. Biomechanical testing

Mechanical testing revealed no differences between the acellular and recellularized groups with respect to yield strength (proximal union 76.6 ± 97.3 MPa versus 113.8 ± 72.3 MPa, $P = 0.50$; distal union 62.8 ± 87.7 MPa versus 69.1 ± 99.9 MPa, $P = 0.91$) or flexural strength (proximal union 86.5 ± 104.9 MPa versus 130.5 ± 79.4 MPa, $P = 0.46$; distal union 77.9 ± 94.0 MPa versus 134.3 ± 124.0 MPa, $P = 0.41$).

3.4. Histology

Histological analysis confirmed evidence of neobone formation on both the acellular and recellularized grafts. Cells in the area of this neobone formation were GFP-negative, suggesting that they were host-derived. In the recellularized grafts no evidence of an inflammatory reaction was seen, despite the heterologous origin of the cells used for recellularization. In these animals, GFP-positive cells were identified in all grafts.

4. Discussion

Critical-size limb defects can result from trauma, tumor resection, or congenital anomalies. Typically, these defects are repaired using either human bone allografts

or vascularized or non-vascularized autografts [12]. While commonly used, these techniques suffer from numerous complications, and have limited applicability in the pediatric setting [13–15].

Within the field of regenerative medicine, there has been widespread interest in the use of scaffolds based on a decellularized extracellular matrix (ECM) [16]. The rationale for using de-cellularized ECM as a scaffold biomaterial is the continued presence of bioactive proteins that promote tissue regeneration. This concept has been recently applied to the construction of osseous grafts in experimental models [5, 17, 18], and clinical experience is beginning to emerge [19]. This bone allograft can provide mechanical strength early in the healing process, allowing for autogenous cell engraftment and vascular invasion [12]. Allogenic bone grafts have been used for many years for the repair of bone defects, however the engineering of these grafts often involves varying degrees of demineralization in order to facilitate processing and clinical use [20, 21]. While subjected to similar cleaning and sterilization steps, allografts stored in bone banks are not commonly formally decellularized [22]. Commercially available allograft bone is also subject to a variety of complications related to the incomplete removal of host cells [23].

Demineralized bone matrix (DBM), a commercially available biomaterial, can be used in a variety of clinical situations as an adjunct to allografting or acellular implants. Engineered as an acid-extruded organic matrix from human bone sources, it is used to induce bone formation and to accelerate healing. DBM alone, however, is not sufficiently rigid to be used for long bone repair [24, 25].

In principle, grafts engineered from simple decellularized bone could offer several advantages over current treatment strategies for critical-size limb defects. Cadaveric bone could be readily available throughout the neonatal and pediatric periods. Grafts engineered from cells seeded to synthetic scaffolds often require many weeks of culture time in order to produce a graft that is structurally sound [1–3], but simple decellularized bone would require a much shorter engineering time. It is also likely that some of the native osteogenic properties of the decellularized bone remain intact, perhaps leading to greater engraftment of host cells in the long term. Indeed, it has been shown experimentally that decellularized bone scaffolds can support mesenchymal stem cell (MSC) adherence and integration in a xenologous model [17]. As they have not been demineralized, the grafts have substantial rigidity, making them ideal for structural repair and minimizing the need for external fixation. In our study, the acellular scaffolds were incubated in the same culture media used for the recellularized grafts in order to constitute proper controls. Such media contained dexamethasone, which has been linked to bone loss and osteoporosis over long term administration [26–29]. On the other hand, it has also been shown that dexamethasone treatment induces proliferation and differentiation of human and murine osteoblast precursors. Specifically, for example, bone morphogenic protein-induced bone formation is significantly enhanced by the systemic short term administration of dexamethasone in mice [30].

We have chosen to investigate the effect of controlled recellularization based on broad experimental evidence that MSCs can improve the structural repair of bony defects [1, 3, 31–33]. We have shown experimentally that MSCs derived from amniotic fluid can be used to engineer osseous grafts amenable to the repair of flat and diploic bone defects, including chest wall and craniofacial deformities [1–3]. Other groups have shown that critical size long bone defects can be repaired using an autologous osteogenic-like tissue engineered from MSCs [34].

For many reasons, our preferred source for MSCs has been amniotic fluid. As an amniocentesis is indicated whenever a structural deformity is diagnosed prenatally, there are no additional procedures required to obtain fetal tissue for autologous tissue engineering, resulting in no additional risk to the mother or fetus. Our group has explored the use of amniotic MSC-based tissue engineering in multiple experimental models of congenital anomalies, not necessarily involving bone repair [1–3, 35–39]. In this first study involving long bone repair, we elected to use a heterologous, rather than autologous, cell source, owing to the combination of a short leporine gestational time (term = 33 d) and the relatively low survival rates in rabbits after fetal intervention, including autologous cell procurement. Much like our previous studies using heterologous amniotic MSCs in rabbits and other species, and despite the heterologous origin of the donor cells in this study, we observed virtually no inflammation in the recellularized grafts, perhaps due to the known immuno-regulatory properties of amniotic MSCs [40–42]. The donor cells survived in all grafts.

There are a number of potential reasons why we did not observe statistically significant differences in the structural or biomechanical properties between the acellular and recellularized grafts. While we cannot rule out type II errors common to large animal models using a relatively small number of subjects per group, the most likely explanation relates to the fact that decellularized, non-demineralized grafts represent such a stable and rigid scaffold that any small differences induced by recellularization were too small to be detected within the power and time frame of this study.

5. Conclusion

The above-mentioned limitations notwithstanding, we could conclude that osseous grafts derived from decellularized, non-demineralized bone undergo adequate remodeling *in vivo* after the repair of critical-size limb defects in a growing leporine model

and that the recellularization of these grafts with amniotic mesenchymal progenitors does not appear to enhance their biomechanical or structural properties appreciably. Simple decellularized, non-demineralized bone grafts could become a practical alternative for pediatric limb reconstruction.

Acknowledgments

The authors would like to thank Ms K Mullen, Ms D Bolgen, Ms C White and A Nedder, DVM for their expert veterinary care.

References

[1] Turner C G, Klein J D, Gray F L, Ahmed A, Zurakowski D and Fauza D O 2012 Craniofacial repair with fetal bone grafts engineered from amniotic mesenchymal stem cells *J. Surg. Res.* **178** 785–90 (Epub 2012/06/05)
[2] Steigman S A, Ahmed A, Shanti R M, Tuan R S, Valim C and Fauza D O 2009 Sternal repair with bone grafts engineered from amniotic mesenchymal stem cells *J. Pediatr. Surg.* **44** 1120–6 (discussion 6. Epub 2009/06/16)
[3] Klein J D, Turner C G, Ahmed A, Steigman S A, Zurakowski D and Fauza D O 2010 Chest wall repair with engineered fetal bone grafts: an efficacy analysis in an autologous leporine model *J. Pediatr. Surg.* **45** 1354–60 (Epub 2010/07/14)
[4] Cherry S R, Biniszkiewicz D, van Parijs L, Baltimore D and Retroviral J R 2000 expression in embryonic stem cells and hematopoietic stem cells *Mol. Cell Biol.* **20** 7419–26
[5] Grayson W L *et al* 2008 Effects of initial seeding density and fluid perfusion rate on formation of tissue-engineered bone *Tissue Eng.* A **14** 1809–20 (Epub 2008/07/16)
[6] Loening A M and Gambhir S S 2003 AMIDE: a free software tool for multimodality medical image analysis *Mol. Imag.* **2** 131–7
[7] Cory E, Nazarian A, Entezari V, Vartanians V, Muller R and Snyder B D 2010 Compressive axial mechanical properties of rat bone as functions of bone volume fraction, apparent density and micro-ct based mineral density *J. Biomech.* **43** 953–60 (Epub 2009/12/17)
[8] Nazarian A, Entezari V, Vartanians V, Muller R and Snyder B D 2009 An improved method to assess torsional properties of rodent long bones *J. Biomech.* **42** 1720–5 (Epub 2009/05/19)
[9] Lai W M, Rubin D and Krempl E 1993 *Introduction to Continuum Mechanics* 3rd edn (Oxford: Pergamon) xiv, p 556
[10] Darrah T H, Prutsman-Pfeiffer J J, Poreda R J, Ellen Campbell M, Hauschka P V and Hannigan R E 2009 Incorporation of excess gadolinium into human bone from medical contrast agents *Metallomics* **1** 479–88 (Epub 2009/11/01)
[11] Sprauten M *et al* 2012 Impact of long-term serum platinum concentrations on neuro- and ototoxicity in Cisplatin-treated survivors of testicular cancer *J. Clin. Oncol.* **30** 300–7 (Epub 2011/12/21)
[12] Follmar K E *et al* 2007 Combined bone allograft and adipose-derived stem cell autograft in a rabbit model *Ann. Plast. Surg.* **58** 561–5 (Epub 2007/04/25)
[13] Shaffer J W, Field G A, Goldberg V M and Davy D T 1985 Fate of vascularized and nonvascularized autografts *Clin. Orthop. Relat. Res.* **197** 32–43 (Epub 1985/07/01)
[14] Storm T R, Cohen J and Newton E D 1996 Free vascularized bone graft *J. Foot Ankle Surg.* **35** 436–9 (Epub 1996/09/01)
[15] Wood M B 1986 Free vascularized bone transfers for nonunions, segmental gaps, and following tumor resection *Orthopedics* **9** 810–6 (Epub 1986/06/01)
[16] Benders K E, van Weeren P R, Badylak S F, Saris D B, Dhert W J and Malda J 2013 Extracellular matrix scaffolds for cartilage and bone regeneration *Trends Biotechnol.* **31** 169–76 (Epub 2013/01/10)
[17] Shahabipour F, Mahdavi-Shahri N, Matin M M, Tavassoli A and Zebarjad S M 2013 Scaffolds derived from cancellous bovine bone support mesenchymal stem cells' maintenance and growth *In Vitro Cell. Dev. Biol. Animal* **49** 440–8 (Epub 2013/05/28)
[18] Grayson W L *et al* 2010 Engineering anatomically shaped human bone grafts *Proc. Natl Acad. Sci. USA* **107** 3299–304 (Epub 2009/10/13)
[19] Hesse E *et al* 2010 Repair of a segmental long bone defect in human by implantation of a novel multiple disc graft *Bone* **46** 1457–63 (Epub 2010/02/16)
[20] Won Y H, Kim S G, Oh J S and Lim S C 2011 Clinical evaluation of demineralized bone allograft for sinus lifts in humans: a clinical and histologic study *Implant Dent.* **20** 460–4 (Epub 2011/10/12)
[21] Wood R A and Mealey B L 2012 Histologic comparison of healing after tooth extraction with ridge preservation using mineralized versus demineralized freeze-dried bone allograft *J. Periodontol.* **83** 329–36 (Epub 2011/07/14)
[22] Holzmann P *et al* 2010 Investigation of bone allografts representing different steps of the bone bank procedure using the CAM-model *Altex* **27** 97–103 (Epub 2010/08/06)
[23] Gross R H 2012 The use of bone grafts and bone graft substitutes in pediatric orthopaedics: an overview *J. Pediatr. Orthop.* **32** 100–5 (Epub 2011/12/17)
[24] Gruskin E, Doll B A, Futrell F W, Schmitz J P and Hollinger J O 2012 Demineralized bone matrix in bone repair: history and use *Adv. Drug Deliv. Rev.* **64** 1063–77 (Epub 2012/06/26)
[25] Babiker H, Ding M and Overgaard S 2013 Demineralized bone matrix and human cancellous bone enhance fixation of porous-coated titanium implants in sheep *J. Tissue Eng. Regen. Med.* (Epub 2013/01/26).
[26] Lane N E 2001 An update on glucocorticoid-induced osteoporosis *Rheum. Dis. Clin. North Am.* **27** 235–53 (Epub 2001/04/05)
[27] Lipworth B J 1999 Systemic adverse effects of inhaled corticosteroid therapy: a systematic review and meta-analysis *Arch. Intern. Med.* **159** 941–55 (Epub 1999/05/18)
[28] Spreafico A *et al* 2006 Osteogenic growth peptide effects on primary human osteoblast cultures: potential relevance for the treatment of glucocorticoid-induced osteoporosis *J. Cell Biochem.* **98** 1007–20 (Epub 2006/06/24)
[29] Weinstein R S, Jilka R L, Parfitt A M and Manolagas S C 1998 Inhibition of osteoblastogenesis and promotion of apoptosis of osteoblasts and osteocytes by glucocorticoids. Potential mechanisms of Their deleterious effects on bone *J. Clin. Invest.* **102** 274–82 (Epub 1998/07/17)
[30] Spiro A S *et al* 2010 Short-term application of dexamethasone enhances bone morphogenetic protein-7-induced ectopic bone formation *in vivo J. Trauma* **69** 1473–80 (Epub 2010/12/15)
[31] Breitbart E A *et al* 2010 Mesenchymal stem cells accelerate bone allograft incorporation in the presence of diabetes mellitus *J. Orthop. Res.* **28** 942–9 (Epub 2010/01/09)
[32] Goshima J, Goldberg V M and Caplan A I 1991 The osteogenic potential of culture-expanded rat marrow mesenchymal cells assayed *in vivo* in calcium phosphate ceramic blocks *Clin. Orthop. Relat. Res.* **262** 298–311 (Epub 1991/01/01)
[33] Mardon H J, Bee J,von der Mark K and Owen M E 1987 Development of osteogenic tissue in diffusion chambers from early precursor cells in bone marrow of adult rats *Cell Tissue Res.* **250** 157–65 (Epub 1987/10/01)
[34] Schubert T *et al* 2013 Critical size bone defect reconstruction by an autologous 3D osteogenic-like tissue derived from differentiated adipose MSCs *Biomaterials* **34** 4428–38 (Epub 2013/03/20)
[35] Fuchs J R *et al* 2004 Diaphragmatic reconstruction with autologous tendon engineered from mesenchymal amniocytes *J. Pediatr. Surg.* **39** 834–8
[36] Kunisaki S M, Fuchs J R, Steigman S A and Fauza D O 2007 A comparative analysis of cartilage engineered from different perinatal mesenchymal progenitor cells *Tissue Eng.* **13** 2633–44

[37] Kunisaki S M et al 2006 Diaphragmatic repair through fetal tissue engineering: a comparison between mesenchymal amniocyte- and myoblast-based constructs J Pediatr. Surg. 41 34–9 (discussion 9)
[38] Gray F L, Turner C G, Ahmed A, Calvert C E, Zurakowski D and Fauza D O 2012 Prenatal tracheal reconstruction with a hybrid amniotic mesenchymal stem cells-engineered construct derived from decellularized airway J. Pediatr. Surg. 47 1072–9 (Epub 2012/06/19)
[39] Kunisaki S M, Freedman D A and Fauza D O 2006 Fetal tracheal reconstruction with cartilaginous grafts engineered from mesenchymal amniocytes J. Pediatr. Surg. 41 675–82
[40] Arinzeh T L et al 2003 Allogeneic mesenchymal stem cells regenerate bone in a critical-sized canine segmental defect J. Bone Joint Surg. Am. 85 1927–35
[41] Barry F P, Murphy J M, English K and Mahon B P 2005 Immunogenicity of adult mesenchymal stem cells: lessons from the fetal allograft Stem Cells Dev. 14 252–65
[42] Gotherstrom C, Ringden O, Tammik C, Zetterberg E, Westgren M and Le Blanc K 2004 Immunologic properties of human fetal mesenchymal stem cells Am. J. Obstet. Gynecol. 190 239–45